Environmental Fluid Mechanics manuscript No.
(will be inserted by the editor)

Dike-Break Induced Flows: a Simplified Model

F. Stilmant · M. Pirotton · P. Archambeau · S. Roger · S. Erpicum · B. Dewals

Received: date / Accepted: date

Abstract A simplified model for the prediction of the steady-state outflow through a breach in an inland dike is presented. It consists in the application of the mass and momentum conservation principles to a macroscopic control volume. A proper definition of the shape of the control volume enables to take the main characteristics of the flow into account and thus to compensate for the extreme simplification of the spatial representation of the model. At the breach, a relation derived from the shallow-water equations is used to determine the direction of the flow. Developments have been guided by numerical simulations and results have been compared to experimental data. Both the accuracy and the domain of validity of the simplified model are found satisfactory.

Keywords Dike break · Simplified model · Control volume · Critical flow

1 Introduction

The failure of inland flood defence installations such as dikes and (mobile) protection walls can bring about considerable damage in the floodplain of a river. Such damage arises either from the dynamic impact of the flood wave or from the static impact of the submerging water [11, 12]. Both impacts depend on the discharge and water depth in the river and on the location and size of the breach. As the predictions of all these parameters are affected by uncertainties, a risk assessment can not rely on a single scenario but must take into account the probabilistic nature of the problem. With this requirement, the use of numerical models based on the shallow-water equations (SWE) to compute flooding events implies high computational costs.

This paper focuses on the static impact, i.e. the extent, of the flood induced by the failure of a flood defence installation (referred to as a 'dike-break induced flow' in the following).

F. Stilmant · M. Pirotton · P. Archambeau · S. Erpicum · B. Dewals
University of Liège, Research unit of Hydraulics in Environmental and Civil Engineering (HECE)
Chemin des Chevreuils, 1, B4000 Liège, Belgium
Tel.: +32-4-3669267
E-mail: f.stilmant@ulg.ac.be

S. Roger
Aachen University, Institute of Hydraulic Engineering and Water Resources Management
Mies-van-der-Rohe-Strasse, 1, D52056 Aachen, Germany

As this static impact depends on the discharge entering the floodplain, the computation of the discharge distribution at a point in the river network where a breach has formed in a dike is the basic hydraulic problem to be solved. The use of a simplified model instead of a classical SWE-based model to compute this distribution greatly reduces the computational time. The derivation of such a simplified model is made easier by two legitimate assumptions: at the timescale of a whole flood event, the first transient phase during which the breach widens is short [1, 14] and the discharge through the breach tends to a steady value [11, 12].

Simplified models have already been developed for similar configurations but they do not apply in this case. For instance, a one-dimensional approach has been developed for side-weirs [6, 7], but we suppose here that the breach has developed on the entire height of the dike, which results in a different behaviour (see Section 5). Moreover, both empirical formulae (e.g. [9]) and simplified models based on macroscopic control volumes [10] have been derived for channel bifurcations, but in the case of a dike break, the flow leaving the main channel is not confined by lateral walls but can spread in all directions. There is therefore a need for a simplified model designed for the specific case of dike-break induced flows, all the more so because general empirical formulae (e.g. [8]) are difficult to derive.

The simplified model presented in this paper has been developed in the frame of a scale model described in Section 2; numerical simulations, described in Section 3, have provided some insight into the characteristics of the flow; Section 4 presents the conceptual model; Sections 5 and 6 then focus on the flow conditions at the breach; the final system of equations is given in Section 7; results are finally compared to experimental data in Section 8 and the domain of validity of the model is discussed.

2 Experimental data

A scale model built at the University of Aachen has been used to study the transient phase [11] and steady state [12, 13] of dike-break induced flows, using both experimental data and numerical simulations.Steady-state discharges through the breach (Q_b) measured on the scale model are used here to assess the performance of the simplified model (results presented in Section 8).

The scale model, presented in Fig. 1a, takes into account the boundary conditions of a dike break, yet with a simple geometry, without bottom slope and with low friction so as to focus on the influence of three parameters:

- the breach width B_b (0.30, 0.50 or 0.70 m – the channel width B_c is constant and equal to 1 m);
- the inflow discharge Q_i (0.100, 0.200 or 0.300 m^3/s);
- the initial water depth h^* in the channel (0.25 to 0.50 m), which depends on the height h_w of the weir at the end of the downstream reach.

The initial state refers to the steady flow in the channel with a closed breach. The experimental set-up is comprehensively described by Briechle [2] and Roger et al. [12].

3 Numerical simulations

In the work of Roger et al. [12], numerical simulations were run to reproduce experimental data measured on the scale model described above. They were based mostly on the finite

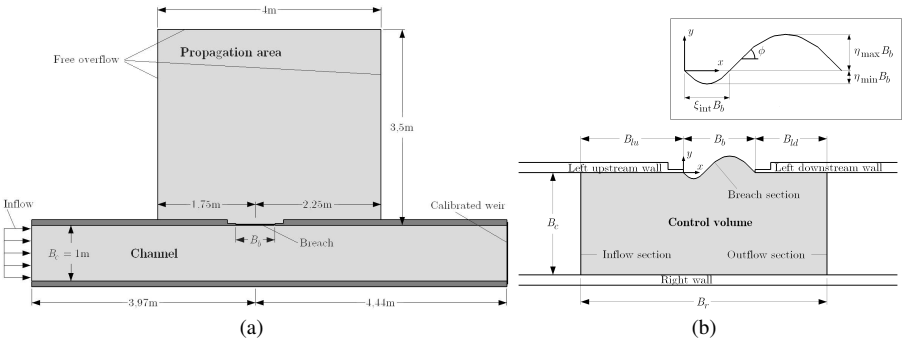

Fig. 1 a) Scale model set-up (adapted from Ref. [2]) - b) Control volume of the simplified model (inset: breach section enlargement)

volume model WOLF 2D (University of Liege), which has also been used here to expand the set of simulated configurations.

WOLF 2D solves the SWE, which are obtained by depth-averaging the equations of mass and momentum conservation. The derivation of the standard form of the SWE relies on two main assumptions, i.e. low vertical velocity (leading to hydrostatic pressure) and uniform flow velocities over the depth. This mathematical model is solved by a finite volume scheme applied on multi-block Cartesian grids. Limited linear variable reconstruction at cell interfaces is used to achieve second-order accuracy in space. Computation of fluxes at cell interfaces is based on a flux vector splitting method [3, 4]. Time integration is performed by means of a dissipative three-step first-order accurate explicit Runge-Kutta algorithm, suitable for the computation of steady flows.

In accordance with Roger et al. [12], the Cartesian grid involved 0.02 by 0.02 m cells. However, for configurations with breach widths of 50 and 30 cm, a refined mesh with 0.01 by 0.01 m cells has been used near the breach. Boundary conditions (inflow discharge, weir equation and free overflow) matched the actual ones as described in Fig. 1a. In particular, the weir equation at the end of the downstream reach required appropriate calibration [12].

In the specific case of the scale model described in Section 2, it was shown that neither bed nor wall friction, nor even turbulence models have a substantial impact on the steady discharge through the breach [12]. As a consequence, and in accordance with the 'base simulations' of Roger et al. [12], present simulations rely on a Manning formula for bed friction (Manning coefficient of 0.015 s/m$^{1/3}$) but neither wall friction nor turbulence model.

4 Conceptual model

We suggest a model based on the integration of mass and momentum conservation on a macroscopic control volume located across the channel near the breach (Fig. 1b). The control volume shows distinctive characteristics which are justified in Sections 5 and 6.

The equations used throughout this paper are the steady-state SWE on a horizontal and smooth bottom:

$$\begin{cases} \partial_x (q\cos\theta) + \partial_y (q\sin\theta) = 0 \\ \partial_x\Big(\dfrac{q^2}{h}\cos^2\theta + \dfrac{gh^2}{2}\Big) + \partial_y\Big(\dfrac{q^2}{h}\sin\theta\cos\theta\Big) = 0 \\ \partial_x\Big(\dfrac{q^2}{h}\sin\theta\cos\theta\Big) + \partial_y\Big(\dfrac{q^2}{h}\sin^2\theta + \dfrac{gh^2}{2}\Big) = 0 \end{cases} \tag{1}$$

The coordinate system is shown in Fig. 1b. In Eq. (1), h (m) is the water depth, q (m^2/s) is the magnitude of the unit discharge and $\theta \in]-;]$ is the flow direction defined by Eq. (2), q_x and q_y being the unit discharges in x and y directions respectively:

$$\begin{cases} q_x = q\cos\theta \\ q_y = q\sin\theta \end{cases} \tag{2}$$

Each line of Eq. (1) can be written as $\partial_x f + \partial_y g = 0$. This system is integrated on the domain A of the control volume, and Green's theorem is applied so as to get a system of equations in which the unknowns are water depths and unit discharges along the boundary $\mathscr{F}^+$ of the control volume ($\mathscr{F}^+$ is oriented anticlockwise):

$$\iint_A (\partial_x f + \partial_y g)\,\mathrm{d}A = 0 \quad \Leftrightarrow \quad \oint_{\mathscr{F}^+} f\mathrm{d}y - g\mathrm{d}x = 0 \tag{3}$$

Basic unknowns of the problem are chosen as water depths and magnitude of unit discharges along the 'inflow' (h_i and q_i), 'outflow' (h_o and q_o) and 'breach' (h_b and q_b) boundaries of the control volume (Fig. 1b and Table 1). Definition of the distribution of these unknowns along the boundaries of the control volume is straightforward, since positions and shapes of the inflow, outflow and breach boundaries, shown in Fig. 1b, ensure constant water depths and magnitude of unit discharge along each of them, as deduced from results of 2D numerical simulations. These numerical results also show that flow directions are parallel to the x axis at the inflow and outflow sections.

Table 1 Unknowns and boundary conditions

Boundary	Location	Unknowns	Boundary condition
'Inflow'	Across upstream reach	h_i, q_i	q_i (prescribed value)
'Outflow'	Across downstream reach	h_o, q_o	$h_o = h_o(q_o)$
'Breach'	Across breach	h_b, q_b	$h_b = h_b(q_b)$

Integration of Eq. (1) on the control volume and application of Eq. (3), leads to following system (coefficients χ and ζ are defined hereafter):

$$\begin{cases} q_i B_c - q_o B_c - \chi_b q_b B_b = 0 \\ \Big(\dfrac{q_i^2}{h_i} + \dfrac{gh_i^2}{2}\Big)B_c - \Big(\dfrac{q_o^2}{h_o} + \dfrac{gh_o^2}{2}\Big)B_c - \chi_{bx}\dfrac{q_b^2}{h_b}B_b = 0 \\ \zeta_r \dfrac{g\left(h_i^2 + h_o^2\right)}{2}B_r - \zeta_{lu}\dfrac{gh_i^2}{2}B_{lu} - \zeta_{ld}\dfrac{gh_o^2}{2}B_{ld} - \chi_{by}\dfrac{q_b^2}{h_b}B_b - \dfrac{gh_b^2}{2}B_b = 0 \end{cases} \tag{4}$$

Coefficient χ_b links the mass flux at the breach to the unknown q_b. Coefficients χ_{bx} and χ_{by} link the advective fluxes at the breach along x and y directions to the ratio q_b^2/h_b. These coefficients take into account the curved shape of the boundary, through the angle $\phi \in]-/2;/2[$ (defined in inset of Fig. 1b), and the varying flow direction (angle θ). They can be expressed as follows, where $\xi = x/B_b$:

$$\chi_b = \int_0^1 \frac{\sin(\theta-\phi)}{\cos\phi}\,\mathrm{d}\xi \tag{5}$$

$$\chi_{bx} = \int_0^1 \cos\theta\,\frac{\sin(\theta-\phi)}{\cos\phi}\,\mathrm{d}\xi \tag{6}$$

$$\chi_{by} = \int_0^1 \sin\theta\,\frac{\sin(\theta-\phi)}{\cos\phi}\,\mathrm{d}\xi \tag{7}$$

Section 6 details how they can be evaluated.

Coefficients ζ_k, where subscript k refers to one of the three wall boundaries of the control volume, denote uneven pressure fluxes along a given boundary. They are defined by:

$$\zeta_k = \frac{2}{g h_{\mathrm{ref},k}^2 B_k}\int_{B_k}\frac{gh^2}{2}\,\mathrm{d}x \tag{8}$$

According to 2D numerical results, the choice of a control volume with a total length of $2B_c + 2\xi_{\mathrm{int}}B_b$ centered on abscissa $x = 2\xi_{\mathrm{int}}B_b$ ensures constant coefficients ζ_k. ξ_{int} is a parameter describing the shape of the critical section, as detailed in Section 6. Table 2 gives the values of length B_k and reference water depth $h_{\mathrm{ref},k}$ for each wall boundary along with coefficients ζ_k deduced from 2D numerical results.

Table 2 Definition of factors involved in Eq. (8)

Wall	Subscript k	$h_{\mathrm{ref},k}^2$	B_k	ζ_k
Right	r	$h_{\mathrm{ref},r}^2 = (h_i^2 + h_o^2)/2$	$B_r = 2B_c + 2\xi_{\mathrm{int}}B_b$	1,00
Left - upstream	lu	$h_{\mathrm{ref},lu}^2 = h_i^2$	$B_{lu} = B_c$	0,95
Left - downstream	ld	$h_{\mathrm{ref},ld}^2 = h_o^2$	$B_{ld} = B_c - (1-2\xi_{\mathrm{int}})B_b$	1,00

Eq. (4) is made up of three equations which involve six unknowns. A closed problem can however be obtained thanks to three boundary conditions, as indicated in Table 1.

5 Characteristics of the flow near the breach

The presence of a breach in one of the side walls of the channel results in a very complex flow in its vicinity. Nevertheless, this flow shows distinctive characteristics, of which the simplified model takes advantage.

5.1 Critical section located across the breach

The set-up of the scale model ensures that the flow in the channel is subcritical (i.e. Froude number $\mathsf{F} = q/\sqrt{gh^3} < 1$), while it becomes supercritical ($\mathsf{F} > 1$) when flowing through the breach [12]. The simplified model is developed based on these observations.

The flow at the breach becomes critical as a result of a minimum in its cross-sectional area and not a maximum in the bottom geometry as in the side-weir problem [5]. This Venturi flume behaviour can easily be deduced from the sketch of the separation line between the flow leaving through the breach and the flow remaining in the channel (Fig. 2a). The flow undergoes a lateral contraction if

$$q_b > q_i \quad \Leftrightarrow \quad \chi_b \frac{B_b}{B_c} < \frac{Q_b}{Q_i}, \tag{9}$$

i.e. if the breach width B_b is not too large compared to the channel width B_c and the percentage of flow deviated through the breach Q_b/Q_i is high enough. Eq. (9) shows that χ_b acts as a contraction coefficient.

When there is no transcritical flow at the breach, the simplified model is not valid. This is discussed in Section 8.

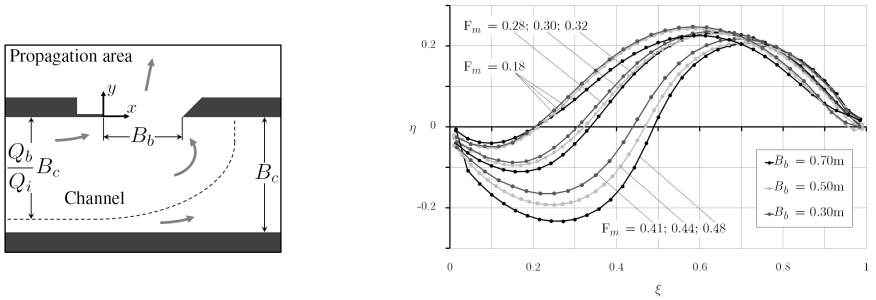

(a) (b)

Fig. 2 Characteristics of the flow near the breach - a) Schematic view of the separation line between the flow that leaves the channel and the flow that does not, as deduced from numerical results (dotted line), and main flow directions (arrows) - b) Critical sections obtained by interpolation of 2D numerical results in different configurations

5.2 Properties of the critical section deduced from numerical results

The computed critical section across the breach takes a distinctive S-shape [12]. Results of 2D numerical simulations plotted in Fig. 2b show that when this shape is drawn in the dimensionless coordinate system (ξ,η) defined as

$$\begin{cases} \xi = x/B_b \\ \eta = y/B_b \end{cases}, \tag{10}$$

it is observed to depend essentially on the momentum of the main flow in the channel, i.e. on the 'mean' Froude number of this flow:

$$\mathsf{F}_m = \frac{1}{2}\left(\mathsf{F}_i + \mathsf{F}_o\right) = \frac{1}{2}\left(\frac{q_i}{\sqrt{gh_i^3}} + \frac{q_o}{\sqrt{gh_o^3}}\right) \tag{11}$$

Beside this distinctive shape, numerical results also indicate that the water depth and the magnitude of the unit discharge are almost constant along the critical section (standard deviations less than 1%). This justifies the choice of the critical section as a boundary of the

control volume for deriving the simplified model. The only flow parameter which varies along this section is the flow direction. Its distribution can be deduced from the SWE, as shown below.

5.3 Properties of the critical section deduced from the shallow-water equations

Consider Eq. (1), in which partial derivatives have been developed and mass conservation has been used to simplify the momentum equations. Dividing by gh enables to obtain:

$$\begin{cases} \cos\theta\partial_x q + \sin\theta\partial_y q - q\left(\sin\theta\partial_x\theta - \cos\theta\partial_y\theta\right) = 0 \\ \left(1-\mathsf{F}^2\cos^2\theta\right)\partial_x h - \mathsf{F}^2\sin\theta\cos\theta\partial_y h - h\mathsf{F}^2\partial_y\theta = 0 \\ \left(1-\mathsf{F}^2\sin^2\theta\right)\partial_y h - \mathsf{F}^2\sin\theta\cos\theta\partial_x h + h\mathsf{F}^2\partial_x\theta = 0 \end{cases} \tag{12}$$

For $\mathsf{F}=1$, these equations become

$$\begin{cases} \cos\theta\partial_x q + \sin\theta\partial_y q = 0 \\ \partial_x\theta = \dfrac{1}{h}\cos\theta\left(\sin\theta\partial_x h - \cos\theta\partial_y h\right) \\ \partial_y\theta = \dfrac{1}{h}\sin\theta\left(\sin\theta\partial_x h - \cos\theta\partial_y h\right) \end{cases} \tag{13}$$

To interpret these relations, let $\mathbf{e}_1 = \cos\theta\mathbf{e}_x + \sin\theta\mathbf{e}_y$ be the unit vector in the direction of the flow and let $\mathbf{e}_2 = -\sin\theta\mathbf{e}_x + \cos\theta\mathbf{e}_y$ be the unit vector in the normal direction. Eq. (13) can then be rewritten in two vectorial equations:

$$\nabla q\cdot\mathbf{e}_1 = 0 \tag{14}$$

$$\nabla\theta = -\left(\frac{\nabla h}{h}\cdot\mathbf{e}_2\right)\mathbf{e}_1 \tag{15}$$

The stationary SWE state that, for a continuous critical flow on a horizontal frictionless bottom,

- the gradient of the magnitude of the unit discharge is either nil or normal to the flow direction;
- the gradient of the flow direction is parallel to the flow direction and its magnitude is given by the projection of the water depth gradient in the direction normal to the flow.

6 Modelling of the flow through the breach

At the breach, the boundary of the control volume follows the critical section. This choice offers several advantages. First, 2D numerical simulations show that q is constant along the critical section, which is consistent with Eq. (14). Since $\mathsf{F}=1$ everywhere on the critical section, a constant q implies a constant h along the same section. Moreover, the distribution of θ can be derived from Eq. (15) and the critical regime can be used as a boundary condition (see Table 1). However, this approach implies a modelling of the dimensionless shape of the critical section, which is Froude dependent.

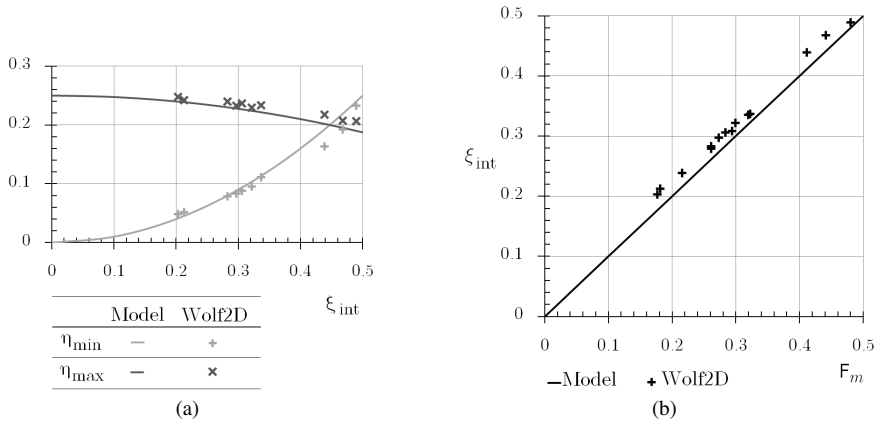

Fig. 3 Modelling of the parameters of the critical section: a) $\eta_{\min}$ and $\eta_{\max}$ as functions of ξ_{int} - b) ξ_{int} as a function of F_m

6.1 Modelling of the critical section

The dimensionless shape of the critical section can be described by two parabolae characterized by only three parameters: ξ_{int}, $\eta_{\min}$ and $\eta_{\max}$, as shown in the inset of Fig. 1b). Two relations between them can be deduced from 2D numerical results (Fig. 3a):

$$\eta_{\min} = \xi_{\text{int}}^2 \tag{16}$$

$$\eta_{\max} = \frac{1}{4}\left(1 - \xi_{\text{int}}^2\right) \tag{17}$$

Based on 2D numerical results, parameter ξ_{int} may be related to the mean Froude number F_m of the flow in the channel as follows (Fig. 3b):

$$\xi_{\text{int}} = \mathsf{F}_m \tag{18}$$

The two parabolae which define the shape of the critical section give the angles ϕ needed to define coefficients χ_b, χ_{bx} and χ_{by} in Eqs. (5)-(7). Flow directions are still to be defined, as detailed in next subsection.

6.2 Distribution of flow directions along the critical section

Eq. (15) can be used to calculate the profile of the flow directions by finite differences starting from a point where θ is known. For this purpose, Eq. (15) is projected on the critical section, i.e. in the direction given by angle ϕ. As h is constant along the critical section, ∇h is perpendicular and the projection gives:

$$\mathrm{d}_\xi \theta = \|\nabla h\| \frac{B_b}{h} \frac{\cos^2(\theta - \phi)}{\cos\phi} = K \frac{\cos^2(\theta - \phi)}{\cos\phi} \tag{19}$$

In this equation, parameter K stands for $\|\nabla h\| B_b/h$, where $\|\ldots\|$ is the magnitude of a vector.

Eq. (19) is applied assuming that $\theta = 0$ at the upstream edge of the critical section and K is constant along the critical section (but its value is a priori unknown). Fig. 4a shows

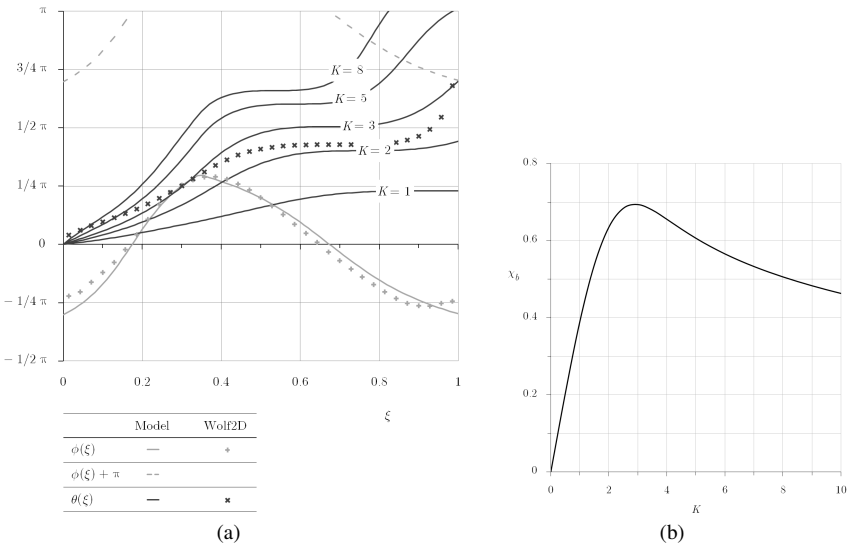

(a) (b)

Fig. 4 Parametrical study of the influence of parameter K on - a) the distribution of angle θ along the critical section - b) coefficient χ_b (example for $\mathsf{F}_m = 0.32$)

different flow direction profiles which can be obtained with different values for K. Most of these distributions involve some points where Eq. (20) is *not* verified:

$$\phi(\xi) \leq \theta(\xi) \leq \phi(\xi) + \tag{20}$$

The efficiency of the critical section in evacuating a discharge Q_b for a given head $H_b = h_b + q_b^2/(2gh_b^2)$ is reduced by these points at which flow enters the channel instead of leaving it. Coefficient χ_b is an indicator of this efficiency since

$$Q_b = \chi_b q_b B_b = \frac{2}{3}\frac{\chi_b}{\sqrt{3}}\sqrt{2g}H_b^{3/2}B_b \tag{21}$$

For a given critical section, i.e. for a given ξ_{int}, the distribution of θ is therefore chosen so as to maximize χ_b (Fig. 4b).

6.3 Computation of coefficients χ_b, χ_{bx} and χ_{by}

Parameter ξ_{int} sets the shape of the critical section, which, in turn, gives the distribution of flow directions; once the distributions of ϕ and θ are known, Eqs. (5)-(7) give the values of coefficients χ_b, χ_{bx} and χ_{by}.

Fig. 5a compares the values given by this method with the values given by the interpolation of WOLF 2D results. At low ξ_{int} (i.e. low F_m), these three coefficients are underestimated by the present model. It can be shown that this is mainly due to the assumption of a constant K, i.e. a constant $\|\nabla h\|$ along the critical section. This hypothesis is however kept for simplicity. For $\xi_{\text{int}} > 0.4$, coefficients are overestimated, which means that the values of q_b and h_b given by Eq. (4) are underestimated. Underestimation of q_b reduces the domain of validity of the simplified model described by Eq. (9).

7 System of equations and numerical scheme

Eq. (4) is solved by a pseudo-unsteady scheme:

$$\begin{cases} \partial_t h_i = \dfrac{1}{A}\left[q_i B_c - q_o B_c - \chi_b q_b B_b\right] \\ \partial_t q_o = \dfrac{1}{A}\left[\left(\dfrac{q_i^2}{h_i} + \dfrac{g h_i^2}{2}\right)B_c - \left(\dfrac{q_o^2}{h_o} + \dfrac{g h_o^2}{2}\right)B_c - \chi_{bx}\dfrac{q_b^2}{h_b}B_b\right] \\ \partial_t q_b = \dfrac{1}{A}\left[\left(\zeta_r \dfrac{B_r}{2} - \zeta_{lu} B_{lu}\right)\dfrac{g h_i^2}{2} + \left(\zeta_r \dfrac{B_r}{2} - \zeta_{ld} B_{ld}\right)\dfrac{g h_o^2}{2} - \chi_{by}\dfrac{q_b^2}{h_b}B_b - \dfrac{g h_b^2}{2}B_b\right] \end{cases} \tag{22}$$

An integration of the *unsteady* SWE on the domain A of the control volume would involve time derivatives of, respectively, the mean water depth and the mean specific discharges in x and y directions. In Eq. (22), these mean values are replaced by the three unknowns h_i, q_o and q_b because the aim is not to compute a transient phase, but simply to converge to a steady flow starting from an arbitrary initial condition.

Boundary conditions, which are simple algebraic relations, are solved at each pseudo-time step to give the values of the unknowns q_i, h_o and h_b:

$$q_i = \frac{Q_i}{B_c} \tag{23}$$

$$q_o = \frac{2}{3}\left(0.657 + 0.084\frac{h_o - h_w}{h_w}\right)\sqrt{2g}\,(h_o - h_w)^{3/2} \tag{24}$$

$$q_b = \sqrt{g h_b^3} \tag{25}$$

Discharge Q_i is a parameter of the problem. Eq. (24) is the weir relation calibrated for the weir at the end of the channel as given by Briechle [2] (h_w is the crest heigth). A more rigorous relation would imply a 1D computation of water depths along the downstream reach of the channel but this proved to be unnecessary in present case (low friction and short reach) and Equation (24) is kept here for clarity.

The time-integration algorithm is a three-step first-order accurate Runge-Kutta scheme.

8 Results

In Fig. 5b, the ratio Q_b/Q_i is plotted against the initial Froude number F^*, which is obtained from the initial specific discharge $q^* = q_i$ and water depth h^*, given by substituting q^* for q_o in Eq. (24).

Experimental data and 2D numerical results are both presented as reference points for the simplified model. Absolute differences of 0.06 can be observed between measured and computed Q_b/Q_i ratios (corresponding *relative* differences less or equal to 11%). According to Roger et al. [12, 13], the underestimation of the discharge through the breach is due to the underlying fundamental assumptions of the SWE model used in the 2D numerical simulations.

As for the simplified model, results show good agreement with those from WOLF 2D simulations: absolute differences between results are less or equal to 0.05 (relative differences less or equal to 15%). Deviations with respect to experimental data are slightly higher, with absolute errors up to 0.15 (relative errors up to 17%). These values show that the substitution of the simplified model for the 2D simulations does not reduce excessively the quality of the results with regard to the gain in computational time.

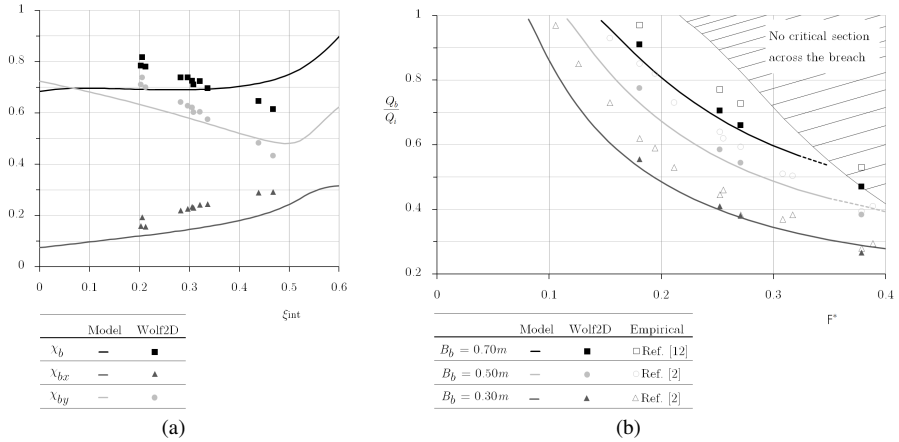

Fig. 5 Comparison of results given by the simplified model with experimental data and/or results given by WOLF 2D: - a) χ_b, χ_{bx} and χ_{by} coefficients as functions of ξ_{int} - b) Q_b/Q_i ratio as a function of the initial Froude number F^* for different breach widths

The domain of validity is however reduced. The present model remains valid provided that a contraction of the deviated flow takes place at the breach (see Section 5). For ranges of parameters for which this effect is not reproduced by the model (i.e. $q_b \leq q_i$), the solutions predicted by the model are not valid (hatched area in Fig. 5b).

Another limitation of the simplified model is linked to the overestimation of coefficients χ_b, χ_{bx} and χ_{by} for $\xi_{\text{int}} > 0.4 - 0.5$ (Fig. 5a). In Fig. 5b, solid lines indicating the results of the model are replaced by dotted lines for configurations in which $\xi_{\text{int}} = \mathsf{F}_m > 0.5$. The effect on the ratio Q_b/Q_i is not important, nevertheless it leads to an overestimation of the hatched zone in Fig. 5b.

9 Conclusion

A simplified model, based on a macroscopic control volume, has been developed for the prediction of the ultimate steady-state outflow through a dike breach. The absence of any space discretisation has required the definition of a proper shape for the control volume, so as to take advantage of the main characteristics of the flow, as disclosed by 2D numerical simulations, and of mathematical simplifications of the shallow-water equations on the critical section.

In view of its simplicity, this model compares well with numerical simulations, which it is intended to replace, and experimental data. Its domain of validity has been investigated focusing on its main underlying assumption, i.e. a critical section crossing the breach, and has been shown to cover a wide range of fluvial conditions.

The experimental set-up used is well-suited for the study of the advective effects incorporated in the simplified model. For real-world applications however, friction and bottom slope terms should be added in the system of equations, as their effects would become more significant. Similarly, it is worth verifying the behaviour of the simplified model in configurations with larger B_c/B_b and B_b/h ratios.

References

1. Aureli F, Mignosa P (2004) Flooding scenarios due to levee breaking in the po river. Water Management 157:3–12
2. Briechle S (2006) Die flächenhafte ausbreitung der flutwelle nach versagen von hochwasserschutzeinrichtungen an fließgewässern (the aerial expansion of flood waves after failure of flood defence installations along rivers). PhD thesis, Rheinisch-Westfälische Technische Hochschule Aachen, (in German)
3. Dewals B, Kantoush S, Erpicum S, Pirotton M, Schleiss A (2008) Experimental and numerical analysis of flow instabilities in rectangular shallow basins. Environmental Fluid Mechanics 8:31–54
4. Erpicum S, Dewals B, Archambeau P, Pirotton M (2010) Dam-break flow computation based on an efficient flux-vector splitting. Journal of Computational & Applied Mathematics 234:2143–2151
5. Hager W (1985) Critical flow condition in open channel hydraulics. Acta Mechanica 54:157–179
6. Hager W (1987) Lateral outflow over side weirs. Journal of Hydraulic Engineering 113:491–504
7. Hager W, Volkart P (1986) Distribution channels. Journal of Hydraulic Engineering 112:935–952
8. Kamrath P, Disse M, Hammer M, Köngeter J (2006) Assessment of discharge through a dike breach and simulation of flood wave propagation. Natural Hazards 38:63–78
9. Krishnappa G, Seetharamiah K (1963) A new method for predicting the flow in a 90° branch channel. La Houille Blanche 18:775–778
10. Ramamurthy A, Tran D, Carballada L (1990) Dividing flow in open channels. Journal of Hydraulic Engineering 116:449–455
11. Roger S, Büsse E, Köngeter J (2006) Dike-break induced flood wave propagation. In: Gourbesville P, et al (eds) 7^{th} International Conference on Hydroinformatics, Nice, France
12. Roger S, Dewals B, Erpicum S, Schwanenberg D, Schüttrumpf H, Köngeter J, Pirotton M (2009) Experimental and numerical investigations of dike-break induced flows. Journal of Hydraulic Research 47:349–359
13. Roger S, Dewals B, Erpicum S, Schwanenberg D, Archambeau P, Köngeter J, Pirotton M, Schüttrumpf H (2010) Hybrid modelling of dike-break induced flows. In: Dittrich A, et al (eds) 5^{th} International Conference on Fluvial Hydraulics (Riverflow), Braunschweig, Germany, pp 523–531
14. Vorogushyn S, Merz B, Lindenschmidt KE, Apel H (2010) A new methodology for flood hazard assessment considering dike breaches. Water Resources Research 46, DOI 10.1029/2009WR008475